Buoyancy-driven convection may switch between reactive states in three-dimensional chemical waves

L. Šebestíková[1,2,*] and M. J. B. Hauser[2]

[1]*Institute of Hydrodynamics, Academy of Science of the Czech Republic, Pod Patankou 30/5, 16612 Praha 6, Czech Republic*

[2]*Institut für Experimentelle Physik, Abteilung Biophysik, Otto-von-Guericke-Universität Magdeburg, Universitätsplatz 2, 39106 Magdeburg, Germany*

(Received 1 July 2011; published 14 March 2012)

Traveling waves in an extended reactor, whose width cannot be neglected, represent a three-dimensional (3D) reaction-diffusion-convection system. We investigate the effects of buoyancy-driven convection in such a setting. The 3D waves traveled through horizontal layers of the iodate–arsenous acid (IAA) reaction solution containing excess of arsenous acid. The depth of the reaction solution was the examined parameter. An increase in the intensity of buoyancy-driven flow caused an increase of the traveling wave velocities. Convection distorted the front of the chemical waves. For layers deeper than $h > 13$ mm, heat release became smaller than heat production causing the emergence of Rayleigh-Bénard convection cells. At the interface, a dependency of wave shape on solution depth was observed. For $h < 7$ mm, the waves adopted a stable V-like shape, while for $h > 13$ mm a parabolic shape dominated. For $7 < h < 13$ mm, both shapes were realized with the same probability. Finally, an intermittent switch between stoichiometric regimes is observed as an unexpected effect of the buoyancy-driven convection. The switch is expressed by iodine enrichment in the product. Hence, the experiments demonstrate that the buoyancy-driven convective flow can cause long-lived, but nevertheless transient, changes in the chemical composition by inducing a local transition between different regimes of the IAA reaction.

DOI: 10.1103/PhysRevE.85.036303 PACS number(s): 47.55.P−, 82.40.Ck, 47.20.Bp, 47.20.Lz

I. INTRODUCTION

During the last thirty years, hydrodynamic instabilities have been investigated at traveling chemical waves [1–15]. In spatially homogeneous liquid systems, thin chemical waves propagate due to coupling between an autocatalytic chemical reaction, diffusion, and free convection. The chemical waves play several roles in such systems. Not only the composition but also the temperature of the reaction solutions, as well as other physical parameters, can be changed during the reaction. Under such conditions, density, surface tension, or viscosity gradients may be formed across the wave front and free convection may develop. [1–4,7,9–13,16,17]. When the reactants and products are miscible solutions, the waves can be regarded as a special kind of physical interface that prevents mixing of the solutions by separating them from each other. Such an interface is mobile, localized, and free of interfacial tension.

An example of such a system is the iodate–arsenous acid (IAA) reaction solution [1–4,10,13,15,16,18–25]. The IAA reaction is composed of two steps [Eqs. (1) and (2)] [1]; their linear combination determines the net reaction stoichiometry and composition of product solutions:

$$IO_3^- + 5I^- + 6H^+ \rightarrow 3I_2 + 3H_2O \quad (1)$$

$$H_3AsO_3 + I_2 + H_2O \rightarrow 2I^- + H_3AsO_4 + 2H^+. \quad (2)$$

Depending on the stoichiometric ratio R

$$R = \frac{[H_3AsO_3]}{[IO_3^-]} \quad (3)$$

(where $[\cdot]$ denotes concentration) of the reactants iodate (IO_3^-) and arsenous acid (H_3AsO_3) three different regimes with respect to product composition are possible: i) stoichiometric excess of arsenous acid (i.e., $R > 3.0$), where iodide (I^-) is the product and iodine (I_2) is an intermediate; ii) stoichiometric excess of iodate ($R < 2.5$), where iodine is the product and iodide is an intermediate; and, iii) when no component is in stoichiometric excess ($2.5 \leqslant R \leqslant 3.0$), arsenous acid and iodate are fully consumed and both iodide and iodine are the products.

In the IAA reaction, the reactants are denser than the products [3]. Therefore, buoyancy-driven flow may develop when dense reactants are stratified above lighter products. The interaction between buoyancy-driven convection and IAA reaction waves was studied for several arrangements. Experiments performed in thin liquid layers placed in Petri dishes [1,16] showed a dependency of the wave velocities on the chosen reaction stoichiometry. Reaction waves were found to i) propagate with a constant velocity for arsenous acid excess, and ii) to accelerate for iodate excess [1,16]. Experiments carried out in capillary tubes reported that both ascending and horizontally propagating waves were affected by the gravity field [3]. This was also confirmed by numerical studies based on reaction-diffusion-convection (RDC) models [4,19,20]. Other experiments performed in thin Hele-Shaw cells and corresponding RDC models studied Rayleigh-Taylor instabilities of ascending IAA reaction waves. The originally flat waves developed fingers that are accompanied by convection rolls [13]. The fingers and their associated convection rolls were shown to grow, split, and merge [10,13,18,21–24]. Recently, Bou Malham *et al.* [15] performed an experimental and theoretical study, where IAA waves propagated horizontally through reaction solutions placed in long, closed

*lenka@n2.cz

cells with a rectangular section. Tilted waves traveling with a constant velocity were observed. The shapes of these waves can be calculated using a parallel flow approximation when the wave velocity is known [15]. Finally, numerical studies were performed with a RDC model using IAA reaction kinetics, where effects of either buoyancy-driven convection [4,14,25] or Marangoni convection [26–28] on vertically oriented wave fronts were examined. Under both conditions, originally vertical wave fronts were tilted and propagated with constant velocities. The velocities were higher than velocities of waves propagating under pure reaction-diffusion (RD) conditions.

This paper reports on experimentally observed buoyancy-driven instabilities of three-dimensional (3D) chemical waves. The waves propagated through horizontal layers (4 mm $< h <$ 20 mm) of the IAA reaction solution containing arsenous acid in stoichiometric excess. The depth of the reaction solution was the examined parameter. Double-diffusive convection is shown to affect pattern formation, as does the depth of the solution layer with respect to the wave velocity. A temporary switch between stoichiometry regimes caused by the convection is discussed.

II. EXPERIMENTS

Experiments were carried out with IAA reaction solutions containing arsenous acid in stoichiometric excess. The net reaction stoichiometry then reads

$$IO_3^- + 3H_3AsO_3 \rightarrow I^- + 3H_3AsO_4. \quad (4)$$

Chemicals used for the experiments were provided by both Sigma-Aldrich and Merck in the quality of analytical standards. The reaction solutions were mixed from stock solutions and their temperature held constant at 21 ± 1 °C. The fresh reaction mixtures contained 0.016*M* Na_3AsO_3, 0.016*M* H_2SO_4, and 0.005*M* $NaIO_3$, thus leading to a stoichiometric ratio of $R = 3.2$. In order to visualize the reaction progress, fresh starch solution (0.06% w/v) was added to the reaction mixture. At the chosen conditions, solutions containing either reactants or final products of the IAA reaction are colorless. The dark blue color, which indicates the presence of iodine, then shows the reaction loci.

The concentrations of reaction species were chosen the same as those used in IAA experiments performed in Hele-Shaw cells [13], in capillary tubes [2,3], and under the influence of an electric current [29–31]. This provides the opportunity to compare the experimental results with previously published results and to profit from measurements of the physical properties (density, *p*H, conductivity) of the reaction mixture. For 0.005*M* $NaIO_3$, Pojman *et al.* [3] determined the total density difference ($\Delta\rho = -1.6 \times 10^{-4}$ g/cm^3) caused by the change of both composition and temperature. Forštová *et al.* [30] measured the *p*H of reactants ($p\mathrm{H}_{\mathrm{reactants}} = 2.14 \pm 0.04$) and products ($p\mathrm{H}_{\mathrm{products}} = 1.92 \pm 0.06$). Although those reaction solutions also contained agar, the *p*H values are very similar to the ones found in the present experiments ($p\mathrm{H}_{\mathrm{reactants}} = 2.11 \pm 0.01$, $p\mathrm{H}_{\mathrm{products}} = 1.92 \pm 0.01$).

The experimental setup is shown in Fig. 1. Channel reactors with rectangular cross sections were made from transparent plexiglass. A cold desk light source illuminated the experiments from below. A mirror was placed above the reactor and inclined by 45°, thus allowing for a simultaneous recording of the lateral and top views using a single CCD camera connected to a computer.

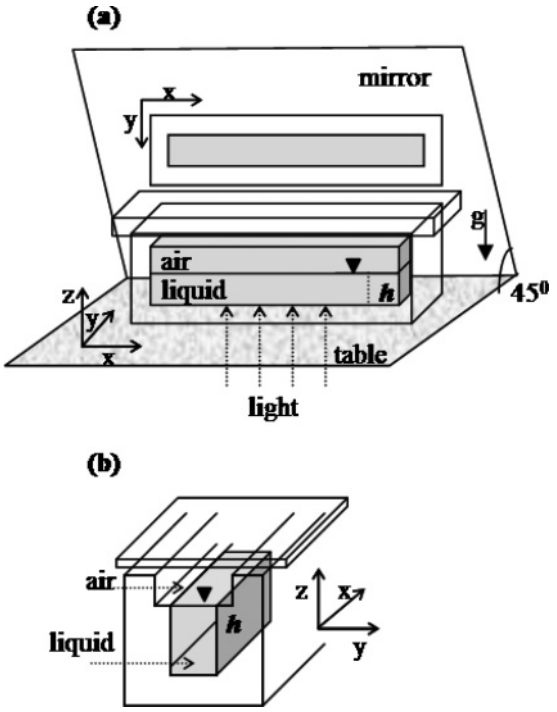

FIG. 1. Experimental setup. (a) The reaction was conducted in a plexiglass channel reactor illuminated from below. Lateral views were directly recorded by the camera, while top views were recorded as an image in a mirror inclined by 45°. (b) Sketch of a side view of the reactor. Reactor size: $L_x = 210$ mm, $L_y = 15$ mm, and $L_z = 30$ mm.

An appropriate volume of freshly prepared reaction solution was placed into the reactor, where the solution formed a liquid layer of depth h. The minimal depth h at which the entire bottom of the reactor was always covered with reaction solution was 4 mm. The maximal h was 20 mm. Immediately after the filling, the autocatalytic reaction was initiated chemically by using a pipet tip filled with 20 μl of reaction products. The tip was carefully and slowly moved toward the reaction solution, where the tip made contact with the interface. The short and very gentle touch did not induce any visible movement of the interface. Diffusion of products from the filled tip into the fresh reactant solution is fast enough to immediately start the autocatalytic reaction at the contact location without any need to actively inject any volume of the product solution. The reactor was then covered by a transparent plexiglass lid. However, an air layer (at least 1 cm thick) remained above the reaction solution [Fig. 1(b)]. Progress of the experiment was recorded from the moment when the reactor was filled with the reaction mixture. The temperature in the reactor and in its environment was kept constant at 21 ± 1 °C by the laboratory air conditioning device.

III. RESULTS

In a channel reactor, the wave development consists of two periods. During the first period, waves are formed. This initial

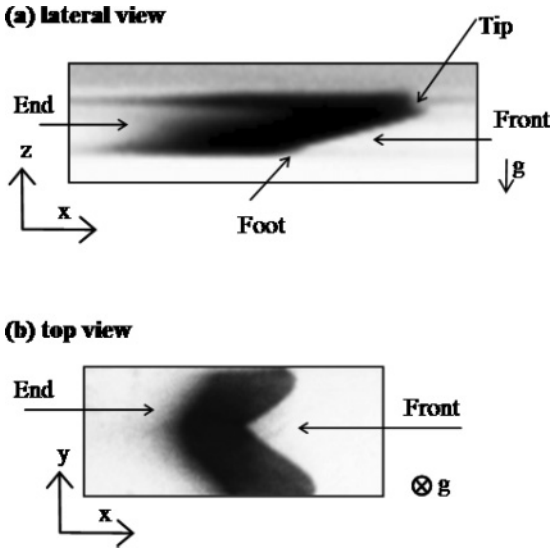

FIG. 2. Definition of the parts of the traveling chemical wave. (a) lateral view, (b) top view. The wave propagates from left to right.

period began with the start of the reaction wave propagation from the edge of the reactor. The initial period, which lasted approximately 200 s, ended when the wave reached the two lateral walls of the reactor. During the second period, the waves traveled through the reactor only in the direction of the x and z axes. Any wave shown in Figs. 2–5 invaded the colorless reactant solution from left to right.

The fully developed wave consists of several parts: a wave front, a wave end, a wave tip, and a wave foot (see Fig. 2). The wave front is defined as the right border between colorless reactants and the dark reaction zone seen in the lateral and top views. Accordingly, the left border of the dark reaction zone determines the wave end. The wave tip and the wave foot are located at the wave front and they are visible in lateral projections only. The tip is the part of a wave front situated close to the reaction-solution–air interface. The wave foot is the lowest part of a wave front, which either propagated towards

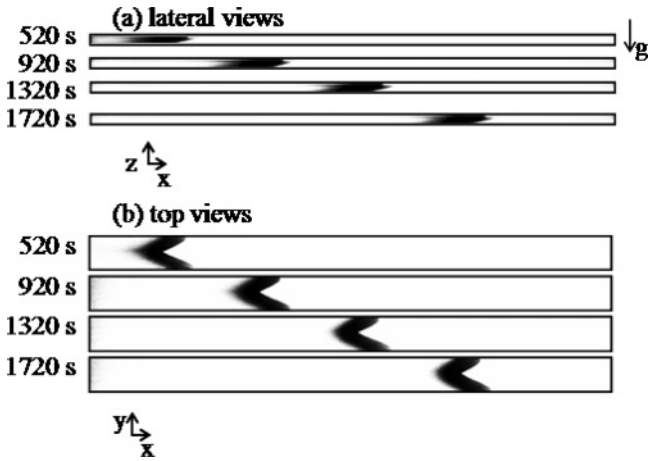

FIG. 3. Traveling wave at a shallow reaction layer of $h = 4$ mm. (a) Lateral views (200×4 mm^2) at different times. The reaction-solution–air interface and the reactor bottom are at top and bottom of images, respectively. (b) Corresponding top views (200×15 mm^2).

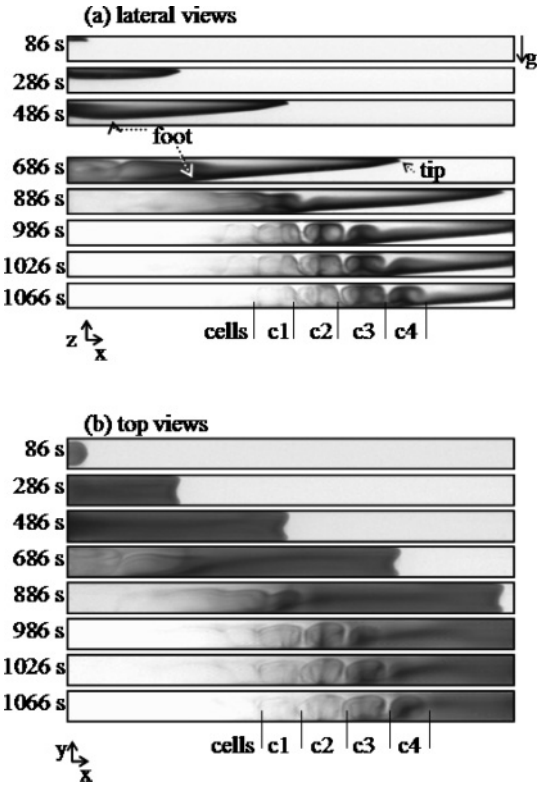

FIG. 4. Traveling wave at a layer depth of $h = 13$ mm. At $t = 86$ s, the wave was still in the first period of development. The other images show wave development during the second period. (a) Lateral views (200×13 mm^2) at different times. The reaction-solution–air interface and the reactor bottom are at the top and bottom of images, respectively. (b) Corresponding top views (200×15 mm^2).

the reactor bottom or was in contact with it. Finally, the wave thickness is the distance between the wave front and the wave end. The wave thickness was determined from the original, nonprocessed images by color intensity analysis. The color intensity was measured along several chosen lines parallel to the reactor bottom or to the reactor side wall, respectively.

Figure 3 shows the development of a wave during an experiment carried out for shallow reaction layers, where $h = 4$ mm. During the initial period, the wave reached the reactor bottom first and the reactor side walls a bit later. During the second period, the wave maintained a constant shape. Seen from the side, the wave front and wave end are both tilted. The wave front is very well defined by a sharp color change, while the end is more fuzzy. The wave thickness was measured at several distances from the reactor bottom. The waves were 23 ± 1 mm thick and the wave thickness was independent on the place of the measurement. Seen from the top, both the wave front and wave end assumed a V-shape. Again, the leading wave front was very sharp, while the end was fuzzy. The wave thickness measured from top views depended on the position of the measurement. The wave is thicker at the side walls (16 ± 1 mm) than at the center of the reactor (11 ± 1 mm). None of these numbers correspond to the wave thickness determined from lateral views, because both the lateral and top views are not thin slices but rather 2D projections of the 3D reality. However, the wave thickness determined from a lateral projection corresponded to the distance between the

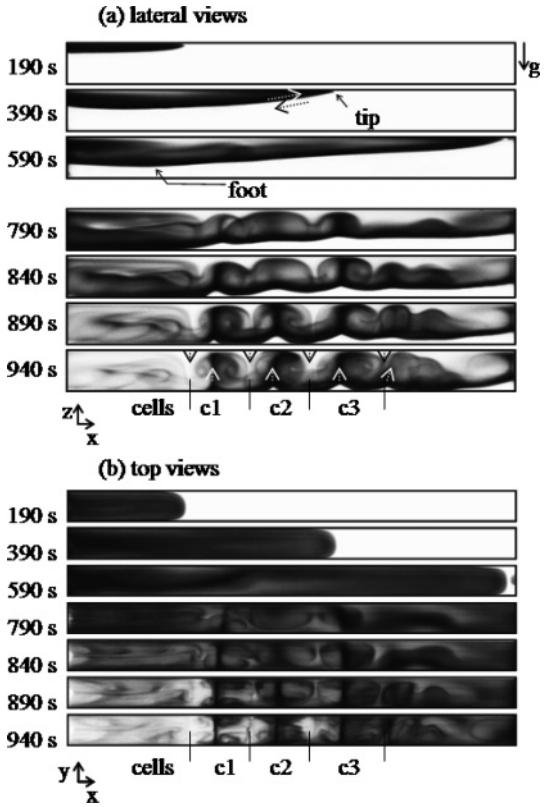

FIG. 5. Traveling wave in a deep reaction layer of $h = 20$ mm. (a) Lateral views (200×20 mm^2) at different times. The reaction-solution–air interface and the reactor bottom are at the top and bottom of images, respectively. Arrows indicate direction of flow in particular places. (b) Corresponding top views (200×15 mm^2).

farthest right position of the wave front and the farthest left position of the wave end seen in top views.

The development of a wave propagating through a 13 mm thick solution layer is depicted in Fig. 4. The formation of a tilted wave front is seen from lateral views. The wave front has the darkest color. The wave foot reaches the reactor bottom after ∼500 s. Once this happened, the entire wave front propagated through the reactor, keeping a tilted shape. In the wake of the wave front, formation of convection rolls was observed. The rolls subsequently rose one after the other from the wave foot [see Fig. 4(a)]. Color intensity analysis shows that the solution returned to colorless only behind the convection cells, indicating that the wave end occurred in the wake of the convection rolls. Hence, the wave extended over a range of ∼10 cm. At the interface, the originally parabolic shape of the wave front developed into a V shape, which was maintained during the second period. The dark color behind the wave front was not homogeneous, but several darker spots were observed there. The positions of the darkest spots corresponded to the loci of the ascending flow.

Figure 5 shows the development of a wave traveling through a 20 mm deep reaction solution layer. The observed patterns were similar to those found at $h = 13$ mm. On lateral views, a tilted wave front and several convection cells can be seen. Between 590 s and 790 s, the tilted wave front becomes undulated due to formation of convection rolls. Three convection cells developed fully. The fourth and the fifth

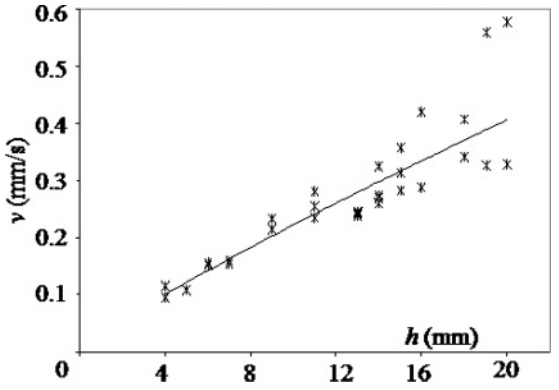

FIG. 6. Dependency of the wave tip velocity on the depth h of the solution layer.

convection cells started to grow but subsequently merged. Seen from above, the wave front had an exclusively parabolic shape. Again several dark and bright spots appeared behind the wave front. At 840 s and later, the dark vertical spots in convection cells c1, c2, and c3 (Fig. 5) corresponded to places where the solution rose.

Finally, the tilted waves propagated through the reactor. Their velocities were evaluated from the lateral projections as the velocities of the wave tips (Fig. 6). The wave-tip velocity increased with the depth h of the reaction solution. At $h = 4$ mm, the wave tip propagated with velocity $v = 0.10 \pm 0.01$ mm/s, which was five times lower than the velocity obtained for a layer depth of $h = 20$ mm ($v = 0.5 \pm 0.1$ mm/s). The results also show that not only the velocities but also their deviations increase with the depth of the solution.

IV. DISCUSSION

For shallow layers of the IAA reaction solution, buoyancy effects on waves were already studied experimentally [3] and theoretically [4,25]. Pojman *et al.* [3] reported that IAA reaction waves assume the shape of tilted thin lines. Tilted waves were also predicted in theoretical studies, where the deformation was explained by the onset of buoyancy-driven convection. [4,25] Moreover, a velocity increase is predicted for augmenting solution layer depths [25]. In our experiments, the formation of tilted wave fronts and the velocity increase were also observed. For deeper solution layers, a higher scattering of wave velocities was obtained. This is most probably related to onset, development, and intensity of the buoyancy-driven flow. Therefore, experiments focused on flow field visualization will be carried out.

Moreover, we observe a series of additional phenomena that have so far not been reported for IAA experiments performed in thin layers [1,3,15,16] and have only recently been predicted, in part, by the RDC models dealing with buoyancy-driven convection [4,25]. These phenomena include formation of multiple convection cells, undulation of tilted wave fronts, the shape of wave fronts seen in top views, and local iodine enrichment in the product solutions. These phenomena are caused by the geometry and the resulting three-dimensional convective flow fields.

The emergence of convection cells and the undulation of the tilted waves reflect the onset of convection. However, 2D RDC

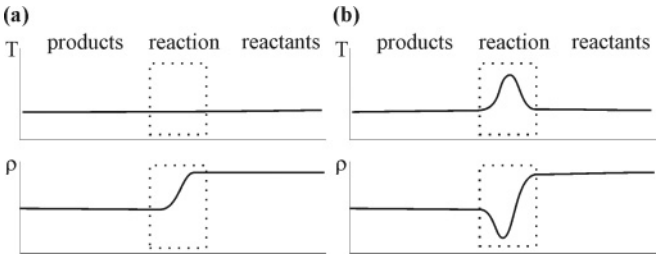

FIG. 7. Sketch of density profiles for (a) isothermal and (b) nonisothermal conditions.

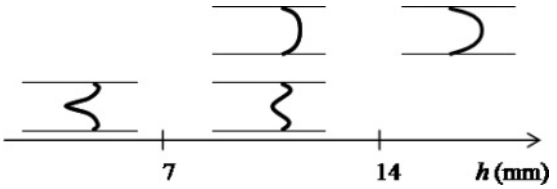

FIG. 8. Sketch of relation between the solution layer depth and the shape of the wave front seen on top views. The wave propagates from left to right.

model studies dealing with solutal density gradients predicted the formation of only a single convection roll co-traveling with the tilted wave [4,25]. Although those models did not consider the exothermic character of the IAA reaction, the heat production during the reaction can play an important role. For the IAA system operated under excess of arsenous acid (at $R = 3.2$), the standard reaction enthalpy is $\Delta H^o = -334$ kJ/mol [3]. The adiabatic temperature rise is then $\sim$0.4 K. Moreover, the thermal and solutal components of the density change are of comparable size and have the same sign, indicating a cooperative effect on the total density change [3]. Although the temperature of the environment of the reactor was kept constant on 21 $\pm$ 1 °C, it is probable that in a 3D reactor the heat release becomes insufficient to keep a constant temperature of the entire reaction solution. Heat will then accumulate close to the reaction wave, causing local temperature increases, which lead to local density decreases [see Figs. 7(a) and 7(b)]. Consequently, two gradients of density could be formed: one between the colder reactants and the hotter products across the reaction wave, and the second between hot products at the reaction zone and the cold products above them. When the difference in densities becomes sufficiently large, Rayleigh-Bénard convection sets in. Hence, the observed convection cells, which were generated in the wake of the wave front, seem to be of Rayleigh-Bénard type. Recently, Rongy *et al.* [14] reported about thermally induced convection rolls in the chlorite-tetrathionate (CT) reaction system. In contrast to the IAA reaction, the CT reaction is strongly exothermic. When the CT reaction is operated under isothermal conditions, the products of the CT reaction are heavier than the reactants. Therefore, the reported dynamics results from a competition between solutal and thermal effects. By contrast, in the IAA reaction system, solutal and thermal effects cooperate. Nevertheless, in the IAA system, tilted waves propagating in an exothermic reaction system seem to be under an effect of double-diffusive convection, leading to the onset of Rayleigh-Bénard convection cells.

Although all wave fronts had shapes with positive curvature during the initial period, as seen from the top views, two types of front shapes were observed during the second period. One of them was V shaped with negative curvature and the other one was a parabolic shape with positive curvature. Figure 8 illustrates the relation between the shape and the solution layer depth h. While shapes with negative curvature dominated in shallow layers ($h < 7$ mm), waves with positive curvature were predominant in deeper solution layers ($h > 14$ mm). For 7 mm $\leqslant h \leqslant$ 14 mm, both types of wave shapes were observed with the same frequency. Formation of single waves with negative curvature is already known for the reaction-diffusion media, where mass transport of some species in one particular direction dominates [32]. Our experiments have shown that a single wave with negative curvature can also exist in a reaction-diffusion-convection medium. One possible explanation for the observed behavior could be a nonhomogeneous layer depth related to naturally formed meniscus. As shown, the wave velocity increased with the layer depth (Fig. 6). Therefore, the wave velocity might be slightly higher very near the reactor side walls, because, due to the meniscus, the solution layer is higher there. However, there is no flow immediately adjacent to the side walls. Therefore, the wave is more advanced at a small distance from the wall before forming the V shape [Fig. 2(b)].

The wave thickness was found to increase with the solution depth. For shallow solutions of a few millimeters depth, iodine accumulation was not observed, as the solution in the wake of the wave remained colorless. For $h > 13$ mm, iodine accumulation in the area behind the leading edge of the wave could already be observed, as seen from the intense color of the solution. This is especially pronounced close to the wave foot. The area remained dark for more than 10 min. Under those conditions it was difficult to accurately estimate the wave thickness because of iodine enrichment, formation of the Rayleigh-Bénard convection cells, and the very fuzzy wave end located behind the rolls. For $h > 15$ mm, the entire wave front and the colorless product solution were not visible simultaneously at the same image. It took several minutes until the dark solution containing iodine became colorless.

The enrichment of iodine in the wake of the wave is an unexpected effect. Since the reaction was operated at stoichiometric excess of arsenous acid (i.e., at $R = 3.2$), the product solution should not contain iodine and, therefore, be colorless. This is indeed what happens in the long time limit (i.e., when all hydrodynamic activity has come to a standstill). However, at shorter time scales (i.e., during the minutes following the passage of the reaction wave) a different behavior is observed: In the wake of the reaction wave the dark color of the product solution, which indicates the presence of iodine, was observed for a significant time. This means that the composition of the product solution was changed, corresponding to a regime where the stoichiometric ratio R assumes a value of $2.5 \leqslant R < 3.0$, thus pointing to a temporary switch in local stoichiometry.

An alteration of the net reaction stoichiometry was already studied for the IAA reaction placed in a gel [29–31]. The stoichiometry switch was controlled by an external electric field imposed on the system. The electric current selectively affected the transport of ionic species and thus caused local

changes in the concentrations of the reacting species leading to a net alteration of the reaction stoichiometry. For excess of arsenous acid, the stoichiometric switch was observed for imposed electric fields $E_{\text{switch}} > 0.76$ V/cm [29,30]. In our experiments, the involved transport processes are diffusion and buoyancy-driven convection. Experiments performed in gels have shown that diffusion cannot cause the net reaction stoichiometry switch [29–31]. Therefore, the buoyancy-driven convection remains as the only source responsible for the iodine enrichment in the product solution. One possible scenario is the following: The convective flow transports small volume elements of the reaction wave into areas in the wake of the reaction. These volume elements are rich in the reaction intermediate iodine. At a given position at the wake of the reaction wave, this may eventually lead to a local accumulation of iodine, such that locally the stoichiometric ratio R is changed. Altered stoichiometries can only be maintained for limited times, since asymptotically both the reaction and the supply of reactants with the predetermined stoichiometry ($R = 3.2$ in the present experiments) drive the system back to normal stoichiometric conditions (i.e., an excess of arsenous acid in our studies).

Interestingly, local and temporal alterations in stoichiometry have already been reported to occur in ternary, reactive media that follow nonlinear reaction kinetics [33–36]. Such local changes in stoichiometry are at the origin of stirring effects studied in continuous-flow stirred tank reactors, and they even affect the critical concentrations where bifurcations between dynamical states take place [33–36].

Finally, we wish to emphasize that the exact mechanism explaining how the buoyancy-driven convection can change local concentrations of reaction species still needs to be elucidated in more detail and also tested in numerical simulations. This opens up a field for both experimental and theoretical research.

V. CONCLUSION

Effects of buoyancy were studied on 3D reaction waves, which propagated through horizontal layers of the IAA reaction solution. Tilted wave fronts and an increase of the wave velocity, which were reported for shallow layers earlier [3,25] were also observed for layers up to 20 mm depth. Undulation of the tilted leading edge of the wave and formation of convection cells were observed and the possible Rayleigh-Bénard nature of the convection cells was discussed. Our results together with results obtained for the CT reaction [14] suggest that formation of Rayleigh-Bénard convection cells is a common property of exothermic autocatalytic reaction systems. Cooperation or competition of solutal and thermal contributions to the total density difference did not change the fact that the Rayleigh-Bénard convection cells develop. The negative curvature of the leading edge of the wave and the iodine enrichment due to a temporary switch of the stoichiometric regime are notable effects, which are caused by the three-dimensionality of the studied RDC system.

The presented experimental results open up avenues of research. Studies focused on i) a detailed analysis of the relation between the layer depth and the observed patterns, ii) temperature field, flow field, and concentration field measurements, and iii) system geometry are currently under way. The results reported here may also stimulate the extension of the current RDC models, for example, implementation of mass balances of the key reactive species such that they may help to understand the switch between stoichiometric regimes observed during the experiments.

ACKNOWLEDGMENTS

We thank Professor S. C. Müller for suggesting the study of buoyancy and Marangoni convection in the IAA reaction system. We acknowledge K. Bohuslavová, Department of Language Studies of the Institute for the Czech Language of the Academy of Sciences of the Czech Republic (ASCR) for linguistic support. The presented results were obtained due to support afforded by Abteilung Biophysik, Otto-von-Guericke-Universität Magdeburg, Germany, by the Czech Science Foundation–Grantová agentura České republiky (GACR) through Grant No. P105/10/0919, and by the Institutional Research Plan N. AV0Z20600510.

[1] A. Hanna, A. Saul, and K. Showalter, J. Am. Chem. Soc. **104**, 3838 (1982).
[2] J. A. Pojman and I. R. Epstein, J. Phys. Chem. **94**, 4966 (1990).
[3] J. A. Pojman, I. R. Epstein, T. J. McManus, and K. Showalter, J. Phys. Chem. **95**, 1299 (1991).
[4] D. Vasquez, J. Littley, J. W. Wilder, and B. F. Edwards, Phys. Rev. E **50**, 280 (1994).
[5] M. J. B. Hauser and R. H. Simoyi, Phys. Lett. A **191**, 31 (1994).
[6] M. J. B. Hauser and R. H. Simoyi, Chem. Phys. Lett. **227**, 593 (1994).
[7] K. Matthienssen and S. Müller, Phys. Rev. E **52**, 492 (1995).
[8] B. S. Martincigh, M. J. B. Hauser, and R. H. Simoyi, Phys. Rev. E **52**, 6146 (1995).
[9] K. Matthienssen, H. Wilke, and S. Müller, Phys. Rev. E **53**, 6056 (1996).
[10] J. Martin, N. Rakotomalala, D. Salin, and M. Böckmann, Phys. Rev. E **65**, 051605 (2002).
[11] D. Horváth, T. J. Bansagi, and A. Tóth, J. Chem. Phys. **117**, 4399 (2002).
[12] T. J. Bansagi, D. Horváth, and A. Tóth, Phys. Rev. E **68**, 026303 (2003).
[13] L. Šebestíková, J. D' Hernoncourt, M. J. B. Hauser, S. Müller, and A. De Wit, Phys. Rev. E **75**, 026309 (2007).
[14] L. Rongy, G. Schuszter, Z. Sinko, T. Toth, D. Horvath, A. Toth, and A. De Wit, Chaos **19**, 023110 (2009).
[15] I. Bou Malham, N. Jarrige, J. Martin, N. Rakotomalala, L. Talon, and D. Salin, J. Chem. Phys. **133**, 244505 (2010).
[16] T. A. Gribschaw, K. Showalter, D. Banville, and I. R. Epstein, J. Phys. Chem. **85**, 2152 (1981).
[17] H. Miike, H. Yamamoto, S. Kai, and S. Müller, Phys. Rev. E **48**, R1627 (1993).
[18] B. F. Edwards, J. W. Wilder, and K. Showalter, Phys. Rev. A **43**, 749 (1991).

[19] J. Huang, D. A. Vasquez, B. F. Edwards, and P. Kolodner, Phys. Rev. E **48**, 4378 (1993).
[20] J. Masere, D. A. Vasquez, B. F. Edwards, J. W. Wilder, and K. Showalter, J. Phys. Chem. **98**, 6505 (1994).
[21] M. Böckmann and S. Müller, Phys. Rev. Lett. **85**, 2506 (2000).
[22] A. De Wit, Phys. Rev. Lett. **87**, 054502 (2001).
[23] M. Böckmann and S. Müller, Phys. Rev. E **70**, 046302 (2004).
[24] A. De Wit, Phys. Fluids **16**, 163 (2004).
[25] L. Rongy, N. Goyal, E. Meiburg, and A. De Wit, J. Chem. Phys. **127**, 114710 (2007).
[26] L. Rongy and A. De Wit, J. Chem. Phys. **124**, 164705 (2006).
[27] L. Rongy and A. De Wit, J. Eng. Math. **59**, 221 (2007).
[28] L. Rongy and A. De Wit, Phys. Rev. E **77**, 046310 (2008).
[29] L. Forštová, H. Ševčíková, M. Marek, and J. H. Merkin, Chem. Eng. Sci. **55**, 233 (2000).
[30] L. Forštová, H. Ševčíková, M. Marek, and J. H. Merkin, J. Phys. Chem. A **104**, 9136 (2000).
[31] L. Forštová, H. Ševčíková, and J. H. Merkin, Phys. Chem. Chem. Phys. **4**, 2236 (2002).
[32] P. K. Brazhnik and V. A. Davydov, Phys. Lett. A **199**, 40 (1995).
[33] G. Dewel, P. Borckmans, and D. Walgraef, Phys. Rev. A **31**, 1983 (1985).
[34] L. Hannon and W. Horsthemke, J. Chem. Phys. **86**, 140 (1987).
[35] A. K. Dutt and M. Menzinger, J. Phys. Chem. **95**, 3429 (1991).
[36] M. J. B. Hauser, D. Lebender, and F. W. Schneider, J. Phys. Chem. **96**, 9332 (1992).